IMA Journal of Complex Networks (2020) Page 1 of 18
doi:10.1093/imaiai/drn000

Modelling the impact of structural directionality on connectome-based models of neural activity

AMELIA PADMORE,
amelia.padmore2013@my.ntu.ac.uk

MARTIN R NELSON
martin.nelson@ntu.ac.uk

NADIA CHUZHANOVA
nadia.chuzhanova@ntu.ac.uk

AND

JONATHAN J CROFTS*
Department of Physics and Mathematics, Nottingham Trent University, Nottingham, NG11 8NS, UK
*Corresponding author: jonathan.crofts@ntu.ac.uk

[Received on 20 August 2020]

Understanding structure–function relationships in the brain remains an important challenge in neuroscience. However, whilst structural brain networks are intrinsically directed, due to the prevalence of chemical synapses in the cortex, most studies in network neuroscience represent the brain as an undirected network. Here, we explore the role that directionality plays in shaping transition dynamics of functional brain states. Using a system of Hopfield neural elements with heterogeneous structural connectivity given by different species and parcellations (cat, *C. elegans* and two macaque networks), we investigate the effect of removing directionality of connections on brain capacity, which we quantify via its ability to store attractor states. In addition to determining large numbers of fixed-point attractor sets, we deploy the recently developed basin stability technique in order to assess the global stability of such brain states, which can be considered a proxy for network state robustness. Our study indicates that not only can directed network topology have a significant effect on the information capacity of connectome-based networks, but it can also impact significantly the domains of attraction of the aforementioned brain states. In particular, we find network modularity to be a key mechanism underlying the formation of neural activity patterns, and moreover, our results suggest that neglecting network directionality has the scope to eliminate states that correlate highly with the directed modular structure of the brain. A numerical analysis of the distribution of attractor states identified a small set of prototypical direction-dependent activity patterns that potentially constitute a 'skeleton' of the non-stationary dynamics typically observed in the brain. This study thereby emphasises the substantial role network directionality can have in shaping the brain's ability to both store and process information.

Keywords: Directionality, network neuroscience, Hopfield model, basin stability

1. Introduction

Recent advances in experimental neuroscience that reconstruct detailed characterisations of both structural and functional connectivity in the human brain have led to the development of realistic large-scale

brain network models (1; 2; 3; 4). Such models typically consist of neural masses, such as the Wilson–Cowan (5) or Jansen–Ritt (6) models, with connectome-based interactions and are capable of generating both healthy and pathological EEG rhythms (6; 7; 8) as well as experimentally observed functional connectivity networks (9; 10; 11). These studies suggest that through indirect network-level interactions, a relatively static structural network can support a wide range of functional connectivity patterns that manifest as transient domains of synchronization across subsets of brain regions.

Dynamical systems analysis provides a powerful framework in which to study rapidly evolving patterns of neurophysiological activity. The brain's resting state, in particular, is of great interest from such a perspective since it has been shown to exhibit exploratory dynamics (12), in which the space of admissible patterns (a.k.a. resting state networks (13; 14)) is continuously traversed over time, resulting in a non-stationary dynamical regime. Such dynamics have been coined Functional Connectivity Dynamics by Jirsa *et al* (15) and are considered a consequence of the mutual presence of heterogeneous network connectivity and highly nonlinear activity dynamics, which in the presence of sufficiently strong noise causes a switching between multiple coexisting attractors (16). The number of admissible brain states is believed to subserve the brain's capability to attain different functional configurations, thus motivating a number of recent studies to analyse the capacity of connectome-based networks to store patterns and create fixed point attractor sets. (See, for example, (17) and references therein.)

Brain networks, however, are inherently directed. Unfortunately, due to current limitations in non-invasive imaging techniques (*e.g.* functional MRI and diffusion tensor imaging) most network models of the brain (including those cited above) do not incorporate directionality, and thus reduce an inherently directed network such as the human connectome to an undirected network. The work of Kale *et al.* (18) highlights the impact that network directionality has in shaping brain networks by performing a network analysis for a range of species and parcellations, for which network directionality is known in both directed and undirected cases. Importantly, they found that the addition of reciprocal edges (*i.e.* rendering directed networks undirected) resulted in larger errors in graph-theoretical measures than the removal of the same number of directed edges, leading, for example, to errors in the classification and identification of network hubs, the ramifications of which are potentially far-reaching due to the important role hub nodes play in healthy brain function (19; 20) as well as neuropsychiatric disorders (21; 22; 23).

The aforementioned work focusses on characterising the effect of network directionality on structural brain networks; however, the extent to which perturbations to the directionality of connections influence neural activity on large-scale connectomes has yet to be addressed. The majority of work in this direction has centred on the dynamics of small circuits, such as network motifs (24). For example, in a series of papers (25; 26; 27), Gollo *et al.* found that synchronisation can be amplified by the presence of just a single reciprocal connection, whilst networks rich in triangle motifs (*i.e.* three node motifs with at least one directed edge between any pair of nodes) can exhibit increased levels of both metastability and multistability via a process known as *frustration* (25). At the network level, a number of studies have attempted to reconstruct directed network topologies from observed network dynamics (28; 29; 30). For example, in (29), functional connectivity matrices were constructed from the temporal activity of a network of phase oscillators and equations relating directed network topology and function were formulated in this idealised scenario. Importantly, the prevalence of phase locked solutions were found to be dominated by the in-degree of the network nodes, and whilst structural properties differed at the local network level, in- and out-degree distributions were found to be qualitatively similar for functional and (inferred) structural networks further highlighting the important relation between structural directionality and neural dynamics.

In this paper we extend work by Golos *et al.* (17) to analyse systematically the effect that network

directionality has on the brain's ability to store network patterns. More specifically, activity of neural subunits is described by a deterministic, graded response Hopfield model (31) with connectivity defined via physiologically relevant structural connectomes across a range of species and parcellations. The capacity of connectome-based networks to store patterns is interrogated by determining large numbers of fixed-point attractor sets for both directed and undirected connectomes (obtained via the addition of reciprocal connections) under systematic variation of model parameters. Moreover, we quantify the robustness of said patterns using the basin stability approach forwarded by Menck *et al.* (32), which uses the basin of attraction to assess a steady state's stability in a probabilistic sense (*i.e.* it provides the likelihood of returning to a steady state under a random (non-small) perturbation). Importantly, our approach enables us to determine the extent to which directed network topology influences multistability within connectome-based networks, as well as allowing us to quantify the affect that directionality has on the robustness of neuronal activity patterns in the brain.

2. Methods

2.1 *Structural connectivity*

Network directionality is a fundamental feature of brain networks, yet due to experimental limitations it is typically omitted from network studies of the brain. Motivated by the study of Kale *et al.* (18), here, we investigate the influence that network directionality has on the information storing capacity of connectome-based networks for a variety of different organisms across a range of scales, including two different parcellations of the Macaque monkey cortex (33), a parcellation of the cat cortex (34) and a representation of the nervous system of *C. elegans*, which is a tiny round worm and the only organism to date for which the entire nervous system is mapped out (35; 36). The Macaque and cat datsets are accessible via the Brain Connectivity Toolbox (37). The *C. elegans* data is the same as that used in (38; 39) and is available from `http://www.biological-networks.org/?page_id=25`.

For the mammalian connectomes, nodes represent some predefined collection of brain tissue and edges encode the presence of long-range connections between pairs of brain regions; whilst for the *C. elegans* connectome, nodes represent individual neurons and edges between nodes represent synapses. For consistency in our experiments, edge weights were discarded (when present) resulting in a binary representation of each of the aforementioned connectomes, yielding a binary connectivity matrix $A \in \mathbb{R}^{n\times n}$ such that $a_{ij} = 1$ if brain region (neuron) i projects onto brain region (neuron) j, and is otherwise zero. To obtain undirected versions of the connectomes all connections were made bidirectional resulting in a symmetric adjacency matrix given by

$$B = \operatorname{sgn}\left(A + A^T\right),$$

where $\operatorname{sgn}(x)$ denotes the sign function, which equals 1 for positive inputs, -1 for negative inputs and is otherwise 0. Below we provide further details of the connectomes studied in this work.

Macaque networks. The first Macaque connectivity network we consider is a representation consisting of $n = 71$ brain regions and $m = 876$ directed edges. The network combines the parcellation of the Macaque visual system due to Felleman and Van Essen (40) with that of Yeterian and Pandya (41), which also includes brain regions within the sensorimotor, motor and superior temporal corticies. The second Macaque connectome is the same as that studied in (39), which is based on three extensive neuroanatomical compilations (40; 42; 43) that collectively cover large parts of the cerebral cortex. It consists of $n = 95$ cortical areas and $m = 2390$ directed edges. The connectivity data for these net-

works were originally collated from the CoCoMac database (33) but we obtained them from the Brain Connectivity Toolbox (37).

Cat network. The matrix representing the cat connectome is that given by Scannell *et al.* (34), which is a collation of numerous studies and deploys the parcellation from (44; 45). This results in a connectome with $n = 52$ brain regions and $m = 818$ directed edges.

C. elegans. The *C. elegans* nervous system considered here has $n = 277$ nodes and $m = 2105$ directed edges (38; 39). This network is derived using electron microscopy and is the only fully mapped nervous system to date. It has two types of connections: *chemical synapses*, which are directed, and *gap junctions*, which we treat as bidirectional since experimental techniques are unable to infer directionality in this case.

Figure 1 displays the four connectomes analysed in this study with reciprocal edges added to form the undirected representation of each connectome highlighted in red and the respective proportion of reciprocal edges stated below each connectome. Basic network statistics for both the empirical connectomes as well as their undirected representations are given in Table 1.

2.2 *Nodal dynamics*

Neural activity is described using a variation of the graded response network model due to Hopfield (31), which is a resistance-capacitance model of cell potential. This results in a dynamic network model consisting of n state variables $x_1, x_2, \ldots, x_n$ each describing the average neural activity within a brain region (or neuron):

$$\tau \frac{\mathrm{d}x_i}{\mathrm{d}t} = -x_i + \sum_{j=1}^{n} w_{ji} g(x_j, \theta), \tag{2.1}$$

with

$$g(x, \theta) = \frac{1}{2}\left(1 + \tanh\left(G(Px - \theta)\right)\right). \tag{2.2}$$

Here, τ is a relaxation time constant and the matrix W represents the normalised adjacency matrix, which is defined as

$$W = \frac{1}{||A||_1} A \in \mathbb{R}^{n \times n}. \tag{2.3}$$

In the above, we make use of the one-norm to ensure that each $x_i \in [0, 1]$, which for a matrix $A \in \mathbb{R}^{n \times n}$ is defined by

$$||A||_1 = \max_j \sum_{i=1}^{n} |a_{ij}| = \max_j k_j^{\text{in}},$$

where k_j^{in} denotes the in-degree of the jth node.

The function $g(x, \theta)$ in (2.2) is a sigmoidal function that represents the input-output relationship of each node. The parameters G and P, which represent node excitability and the ratio of excitation over inhibition respectively, determine, alongside the activation threshold θ, the degree of multistability present within the system (2.1). Here, we follow (17) and define a global activation threshold given by

$$\theta = \frac{1}{2n} \sum_{i,j} w_{ji}. \tag{2.4}$$

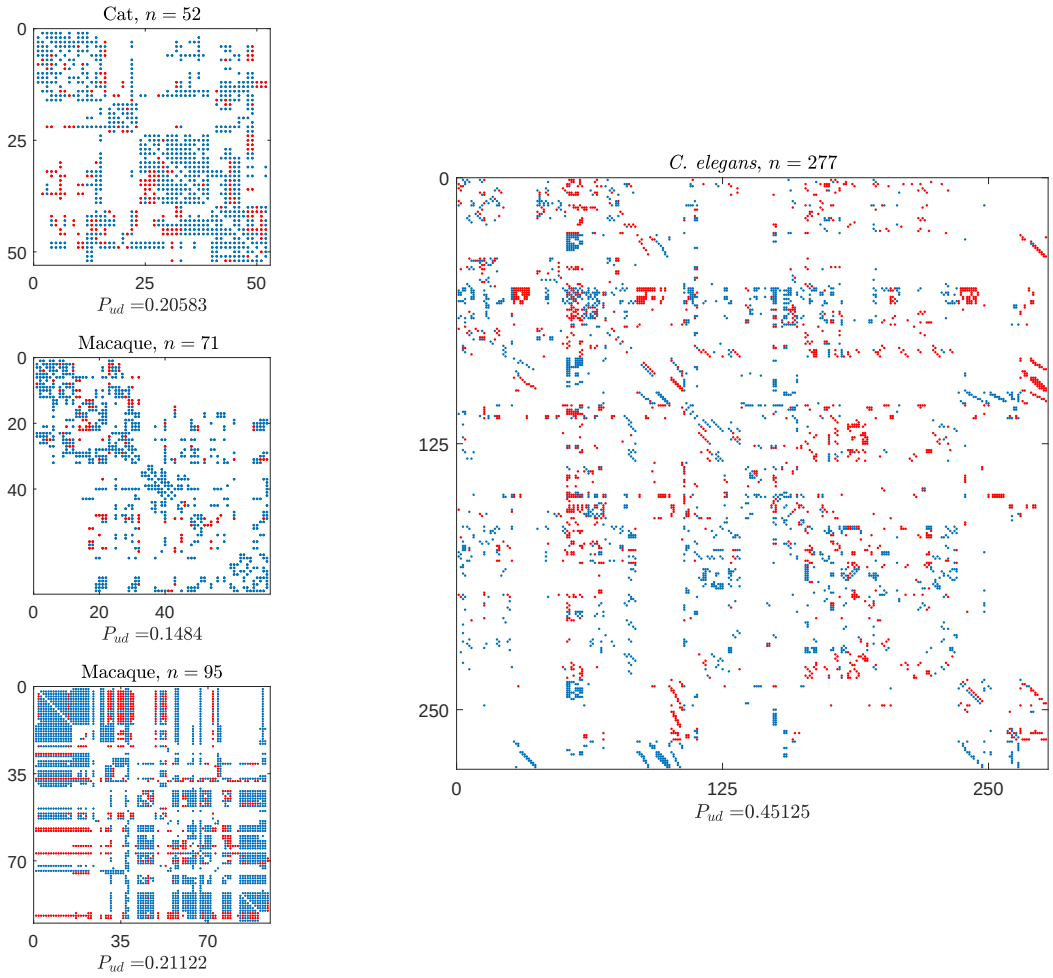

FIG. 1. Spy plots of the adjacency matrices corresponding to the four connectomes studied in this work: two different parcellations of the macaque cortex, the cat cortex and the neuronal network for *C. elegans*. Directed connections are shown in blue. Reciprocal edges added to form the corresponding undirected networks are shown in red. The proportion of reciprocal edges, P_{ud}, is given below each network diagram.

Connectome	Cat		M71		M95		CE	
	D	U	D	U	D	U	D	U
# of edges	818	515	746	438	2390	1515	2105	1918
mean degree	15.73	19.81	10.51	12.34	25.43	32.23	7.60	13.85
# of modules	3	3	4	4	3	2	6	5

Table 1. Network statistics for the original directed connectomes (D) and their undirected representations (U). Here, M71 and M95 denote the Macaque connectomes on 71 and 95 nodes, respectively, whilst CE denotes the *C. elegans* connectome.

The global activation threshold is a simplification of the original Hopfield model since each node uses the same activation threshold. In this simplified setting, nodes with larger in-degree have a larger probability of being active.

The remaining parameters G and P control the dynamical regime. More specifically, G is the system gain which controls the multistability of the system (see, for example, (17)). In our experiments we fixed $G = 10000$ as such large values enhance multistability thus increasing the network's ability to support information. We then investigated the capacity of both directed and undirected connectomes to store patterns under systematic variation of the scaling factor P, since this parameter has previously been hypothesised to play an important role in determining attractor densities.

2.3 *Basin stability*

For each network the dynamics are governed by the Hopfield model in (2.1). To determine the global stability of attractor states, we compute the *basin stability* (32) for each of the steady states of (2.1) as a function of the parameter P. This amounts to estimating the size of the basin of attraction $\mathscr{B}(\mathbf{x}^*)$ of each steady state, $\mathbf{x}^*$, of (2.1). Due to the computational challenges inherent in computing volumes of high-dimensional spaces the basin stability is computed in a relative sense, that is

$$S_{\mathscr{B}(\mathbf{x}^*)} = \mu(\mathscr{B}(\mathbf{x}^*)), \tag{2.5}$$

where μ is an appropriately defined measure over an appropriately chosen domain, Q say, containing all basins of attraction of all attractors. Typically, μ will be proportional to a volume and so $\mu(\mathscr{B}(\mathbf{x}^*)) \in [0,1]$ is a proportion of state space. From a practical point-of-view, suppose that $\mathbf{x}^*$ is an asymptotically stable equilibrium point of (2.1) with basin of attraction $\mathscr{B}(\mathbf{x}^*)$. Then we integrate (2.1) for N initial conditions drawn uniformly at random from Q and count the number, M, of initial conditions that converge to the fixed point $\mathbf{x}^*$, which provides the estimate M/N for the basin stability, $S_{\mathscr{B}(\mathbf{x}^*)}$, of the steady state $\mathbf{x}^*$.

3. Results

3.1 *Network analysis*

Our focus here is on the impact that directionality has on network dynamics; however, for completeness we present a brief overview of the fundamental statistical features of the connectomes introduced in the previous section for both directed and undirected cases. Note that unlike the study by Kale *et al.* (18), that considers a spectrum of perturbed networks comprised of the empirical (directed) connectome at one end and the fully undirected representation of the connectome at the other, we consider only the aforementioned limiting cases here.

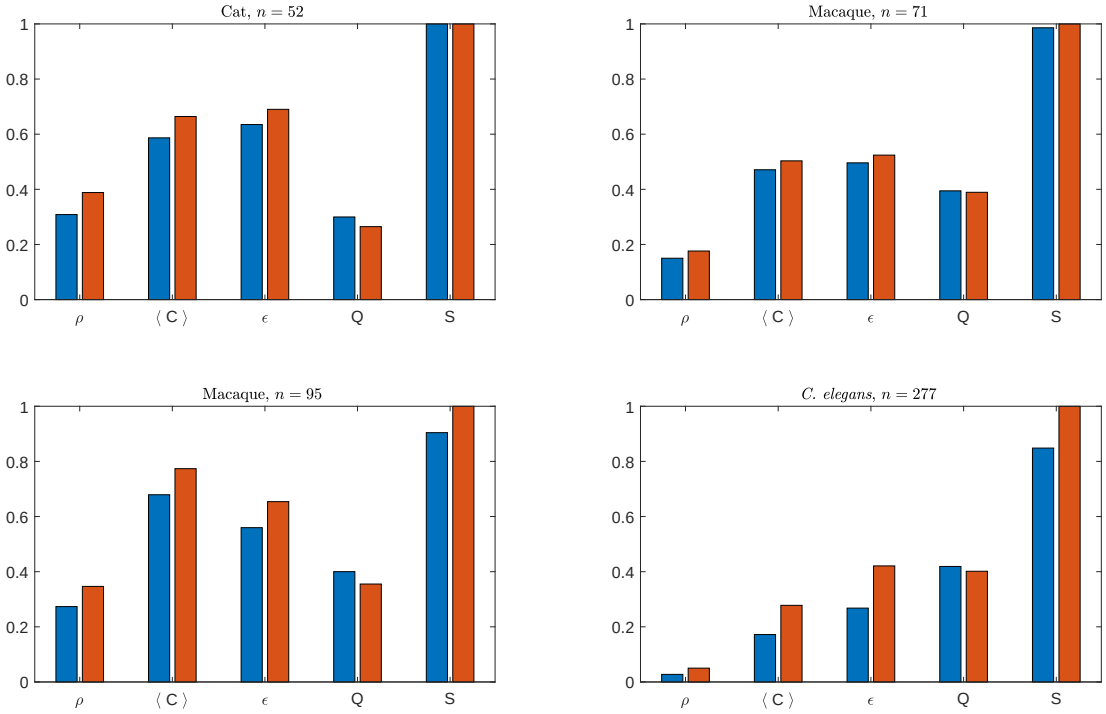

FIG. 2. Network measures for both directed (blue) and undirected (red) connectomes: ρ = density; $\langle C \rangle$ = mean clustering coefficient; ε = efficiency; Q = Newman-Girvan modularity score; and S = size of the giant (strongly) connected component.

Figure 2 shows results of a network analysis for the different connectomes using a range of standard network measures, including the network density ρ; the global Watts-Strogatz clustering coefficient $\langle C \rangle$; and the Newman-Girvan modularity score Q (see, for example, (46) for definitions of these standard network metrics). In addition, since the empirical connectomes are in general not strongly connected, we also compute the relative size, S, of the giant strongly connected component (GSCC) for each connectome, as well as the global efficiency, which is defined as

$$\varepsilon = \frac{1}{n(n-1)} \sum_{i,j,i \neq j} \frac{1}{d(i,j)}.$$

Here $d(i,j)$ is the length of the shortest path between nodes i and j. All network measures were computed using the Brain Connectivity Toolbox (37).

The loss of directionality has the general effect of inflating network measures. For the local metrics considered (*i.e.* the degree and clustering coefficient) this is a direct consequence of the increased density of these networks. Note that whilst the clustering coefficient depends both on degree and interneighbour network connectivity, the addition of reciprocal edges results in a monotonic increase of $\langle C \rangle$. The inclusion of reciprocal edges has a similar inflationary effect on network efficiency since it facilitates shorter (potentially biologically implausible) routes between nodes. Interestingly, network modularity is higher in the empirical connectomes in all cases, which indicates the existence of asymmetric, intermodule connections potentially controlling the flow of neural information between functional modules.

Table 1 shows the number of modules observed for each of the empirical and undirected connectomes corresponding to the modularity scores given in Figure 2. It is noteworthy that in the case of the Macaque connectome on 95 nodes and the *C. elegans* connectome, the removal of network directionality reduces the number of observed modules. We remark that a similar break-down of modular topology due to the existence of false positive connections in undirected brain networks was recently observed in a study by Sporns and Betzel (47). Finally, we note that, with the exception of the cat connectome, all empirical connectomes have GSCCs consisting of less than N nodes; the fraction of nodes in the GSCCs are $0.99, 0.90$ and 0.85 for the Macaque connectome on 71 and 95 nodes and *C. elegans* connectome, respectively.

3.2 *Numerical simulations*

In all of our experiments the time constant and network gain were fixed at $\tau = 10$ and $G = 10000$ respectively. (Such a large value of the gain results in network saturation, at least for the connectomes we analysed.) We then proceeded to investigate the behaviour of the system in (2.1) for different connectomes under variation of the control parameter P. Note that for such large values of G the function in (2.2) approaches a Heaviside function with switching threshold at $x_s = \theta/P$. As the switch approaches zero (*i.e.* in the large P limit) we have that all nodes are active for any non-zero initial condition (as long as the network is strongly connected), and so the system is monostable with almost all initial states converging to the maximal solution, also known as the 'up' state, $x^*_{\mathrm{U}} = W^T\mathbf{1}$. Here $\mathbf{1} = \begin{pmatrix}1, & \ldots, & 1\end{pmatrix}^T$ is the vector of all ones. When the switch is at one (*i.e.* $P = \theta$), the network is in a quiescent 'down' state irrespective of the initial condition. That is, the system is monostable and all initial states converge to the trivial steady state $x^*_{\mathrm{D}} = \mathbf{0}$. For intermediate values of P the system displays multistable behaviour.

In what follows, we choose $P \in [\theta, 10]$ since we have found (experimentally) that the dynamics of (2.1) are unchanged outside this region regardless of the connectome considered. More specifically, for each connectome, we selected 101 equally spaced values of $P \in [\theta, 10]$ and integrated a fixed set of 10^4 initial states drawn at random from the state space $Q = [0,1]^n$. For each distinct fixed point x^* found, we then approximated its basin stability, $S_{\mathscr{B}(x^*)}(P)$, as the proportion of all initial states that converged to x^*. Fixed points were identified by integrating (2.1) for $T = 1000$ using the built-in MATLAB routine `ode45`, with absolute and relative tolerances both set to 10^{-6}. Note that convergence to a fixed point is generally much faster than $T = 1000$ and so the integration was terminated early in this case. To better sample the extremely high-dimensional state space, initial conditions were drawn from a binomial distribution with $x_i(0) \sim \mathrm{Bi}(1, r)$, where r is a random number selected from a uniform distribution over $[0,1]$. In this way, we consider a range of different initial activity patterns. For example, for small r the initial activity pattern has very few 'active' nodes. Conversely, large values of r result in initial activity patterns with large numbers of 'active' nodes.

Figure 3 shows an estimation of the number of final attractors for the four different connectomes as a function of the parameter P. For the three large-scale connectomes (figures 3(a–c)) we find that the number of attractors is relatively small, with a maximum of 4 to 11 different final attractors being observed for any particular P value. Peak pattern variability occurs for $P \approx 1$ for the three large-scale connectomes regardless of whether network directionality is incorporated. In terms of numbers, the empirical cat connectome displays nearly twice as many attractor states at peak variability than its undirected representation, whilst directionality appears to have less of an effect in the case of the two Macaque networks, although the empirical network on 95 nodes displays increased multistability over a broader range of P values. Results for the micro-scale connectome of *C. elegans* are shown in Figure 3(d). Unlike the macro-scale connectomes, we observe large numbers of attractor states for both directed

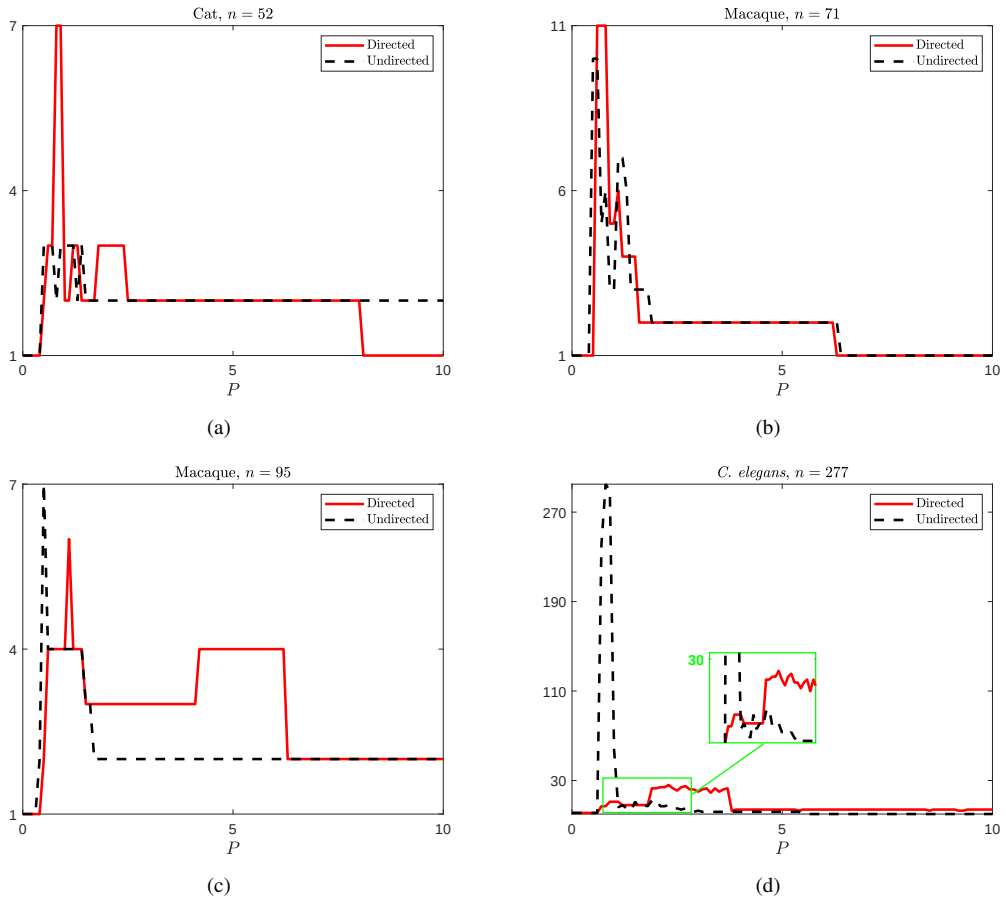

FIG. 3. Estimated attractor numbers as a function of the scaling factor P for each of the connectomes described in Section (2.1).

and undirected connectomes, although significantly more in the undirected case, with approximately 10 times as many attractor states being observed at peak variability. Interestingly, peak variability for the empirical *C. elegans* connectome happens away from $P = 1$, in contrast to the other networks studied. As can be observed from Figure 3(d), the empirical network displays increased multistability over a broader range of P values than its undirected counterpart, peaking for values of P approximately in the plateau range $(2,4)$, although it is worth noting that a local maximum at $P \approx 1$ is also evident. (See the magnified section of Figure 3(d).) These findings are further supported by Table 2, which displays the cumulative number of attractor states (up to $P = 10$) for each of the four connectomes.

Figures 4 and 5 display the basin stability of the steady states of (2.1) as a function of the parameter P for the different connectomes considered in this work. For each value of P, the basin stabilities of each observed steady state are represented as a stacked bar chart with total height 1. Sub-bar heights

Connectome	Cat		M71		M95		CE	
	D	U	D	U	D	U	D	U
Total # of attractors	205	198	204	203	286	223	605	1066

Table 2. Total number of attractors found for the original directed connectomes (D) and their undirected representations (U). Here, M71 and M95 denote the Macaque connectomes on 71 and 95 nodes, respectively, whilst CE denotes the *C. elegans* connectome.

are proportional to the basin stability, $S_{\mathscr{B}(\mathbf{x}^*)}$, and are coloured according to the magnitude of x^* as measured by the one-norm. As expected, for low values of P the system is monostable with all initial states converging to the trivial steady state $x^*_{\mathrm{D}} = \mathbf{0}$ regardless of the connectome. This is evident from the figures since the basin volume consists of a single blue bar. Increasing P sees the emergence of a multistable regime for all connectomes. For the undirected connectomes, regions of parameter space displaying high levels of multistability (*i.e.* more than two attractor states) were roughly contained within the interval $(0.5, 1.5)$, whilst for the empirical connectomes the multistable regime is significantly more widespread. As P is further increased the multistability systematically decreases until only two solutions remain: the trivial steady state, x^*_{D}, and the maximal solution, x^*_{U}, although the basin of attraction for the trivial steady state diminishes rapidly, as expected. We remark that for networks that are only weakly connected, initial states exist that do not converge to the state x^*_{U} regardless of the size of P; however, these solutions are rarely met in practice and so have negligible basins of attraction.

As expected the basin stability plots for the cat connectome differ significantly between the undirected and empirical connectomes. At peak variability the empirical connectome has seven different attractor states each with appreciable basins of attraction, whereas the undirected connectome is essentially bistable with almost all initial conditions converging either to the quiescent state, x^*_{D}, or to a highly active state (*i.e.* one such that $x^* \approx x^*_{\mathrm{U}}$) regardless of the choice of P. A similar feature is observed for both the Macaque networks, in that solutions with intermediate activity tend to have relatively small basins of attraction in the undirected representations. Solutions for the empirical Macaque connectomes, however, exhibit various levels of neural activity as well as an increase in their respective domains of attraction.

The basin stability plots for *C. elegans* (Figure 5) are more complex than those of the mammalian connectomes due largely to the sheer number of solutions determined; however, we still observe broadly similar characteristics to the large-scale networks. Solutions for the undirected connectome are more 'active' on average, whilst multistability is prevalent across significantly larger regions of parameter space for the empirical network. Also, whilst the attractor set for the undirected *C. elegans* connectome consists of up to 295 activity patterns (for any particular P value), a considerable amount of redundancy exists, with many solutions being either very similar (in norm) or possessing negligible domains of attraction. Note that we have performed a clustering analysis (experiments not shown) and determined a small number (3–10 in the multistable regime) of principal modes, or clusters in the attractor landscape, whose significance can be quantified using the combined basin stabilities of the clustered states. Importantly, such dimensionality reduction techniques enable us to characterise large, complex attractor sets, such as that obtained for the *C. elegans* connectome, using just a small number of prototypical activity patterns. Deploying the same technique for the empirical connectome results in 3–5 different prototypical network patterns for values of P in the multistable regime. Importantly, this result suggests that despite the dramatic quantitative differences observed between the undirected and empirical connectomes (see Figure 3(d)), the number of sustainable patterns, whilst larger in the undirected connectome, remains small in both cases.

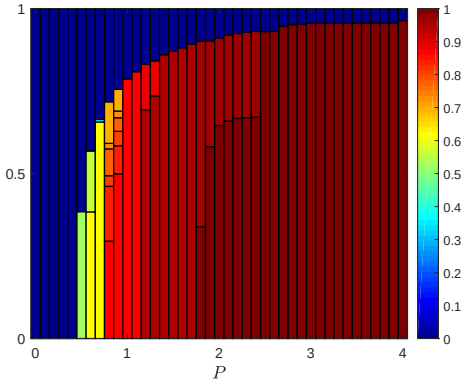

(a) Cat, directed

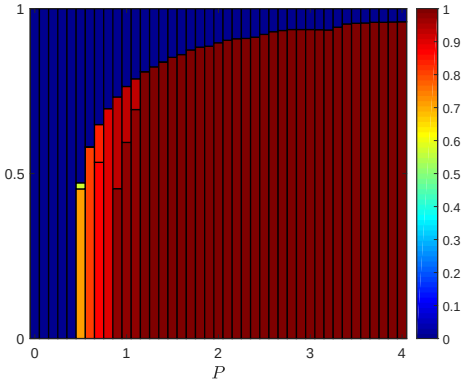

(b) Cat, undirected

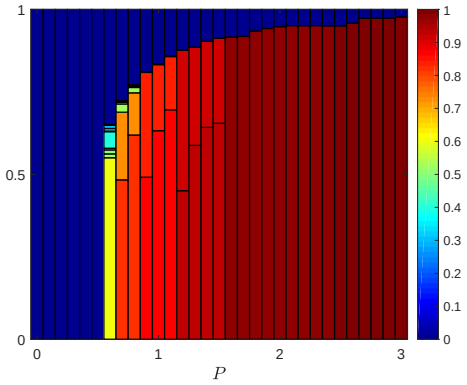

(c) Macaque, $n = 71$, directed

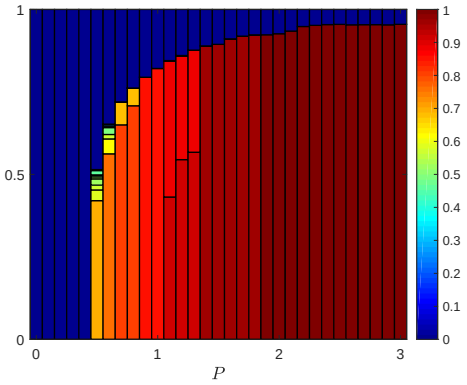

(d) Macaque, $n = 71$, undirected

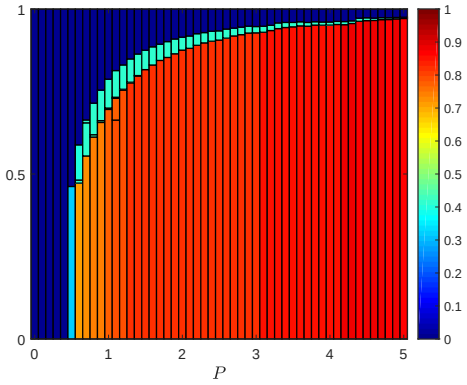

(e) Macaque, $n = 95$, directed

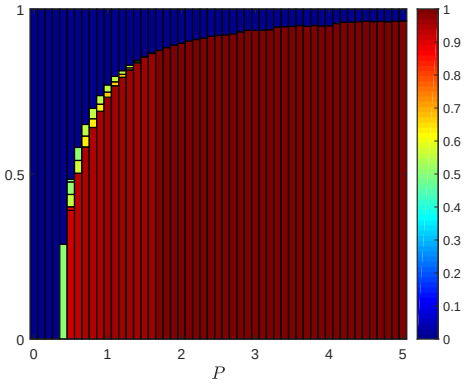

(f) Macaque, $n = 95$, undirected

FIG. 4. Basin stability of the Hopfield neuronal model as a function of the scaling factor, P, for the three large-scale mammalian connectomes considered in this work. (a, b), (c, d) and (e, f) display results for the directed and undirected connectomes of the respective parcellations of the cat and Macaque (on 71 and 95 nodes, respectively) cortex. Each solution is coloured according to its magnitude as measured by the one-norm.

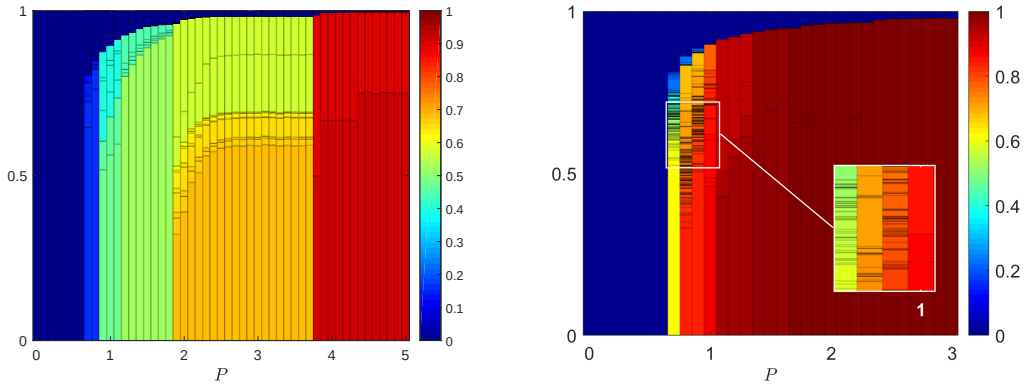

(a) *C. elegans*, directed (b) *C. elegans*, undirected

FIG. 5. Basin stability of the Hopfield neuronal model as a function of the scaling factor, P, for the *C. elegans* neuronal network. (a) and (b) give results for the directed and undirected neuronal networks, respectively. Each solution is coloured according to its magnitude as measured by the one-norm.

In Figure 6 we show an example of a typical set of final activation patterns for the empirical connectome of the Macaque monkey on 95 nodes along with their respective basin stabilities. We display only those solutions with a basin stability score of at least 5% since such network patterns are more likely to be sustainable as they are less sensitive to perturbations arising due to neuronal noise. Figures 6(a, d) display the quiescent state and a high activity state (which are permissible in both empirical and undirected connectomes), whilst figures 6(b, c) show two different intermediate states in which neuronal activity strongly reflects the modular organisation of the Macaque cortical network – a structure that is particularly evident in the spy plot in Figure 1. The two active modules observed in figures 6(b, c) are the same as those in (48) with the one in 6(b) consisting of brain regions belonging to visual pathways (*e.g.* primary visual cortices (V1, V2, V3 and V4), Frontal eye field (FEF), *etc*) serving perception and action (49), whilst the second module is formed of brain regions of importance to the control of movement (*e.g.* supplementary motor area (SMA) and premotor and visuomotor cortices (Brodmann areas 6 and 7)) as well as prefrontal areas responsible for decision making (*e.g.* orbitofrontal cortex (Brodmann areas 11 and 12)). We remark that whilst similar intermediate states (as those shown in figures 6(b, c)) exist for the undirected Macaque connectome, the frequency with which they are observed is greatly diminshed due to the reduction in their respective basins of attraction. As a final note, we emphasise that the modular patterns displayed in Figure 6 are representative of configurations observed across all four connectomes studied here (results omitted for brevity), thus implicating directed network modularity as a key ingredient in the formation of neural patterns.

4. Discussion

In this paper, we have investigated the influence of directed network topology on the activation dynamics of connectome-based networks for a range of species, including the cat, Macaque monkey and *C. elegans* round worm. Whilst network directionality is typically ignored in network investigations of the brain (due largely to limitations in experimental neuroscience), our analysis indicates that it can have a profound effect on network dynamics, both in terms of the number of attractor states observed and

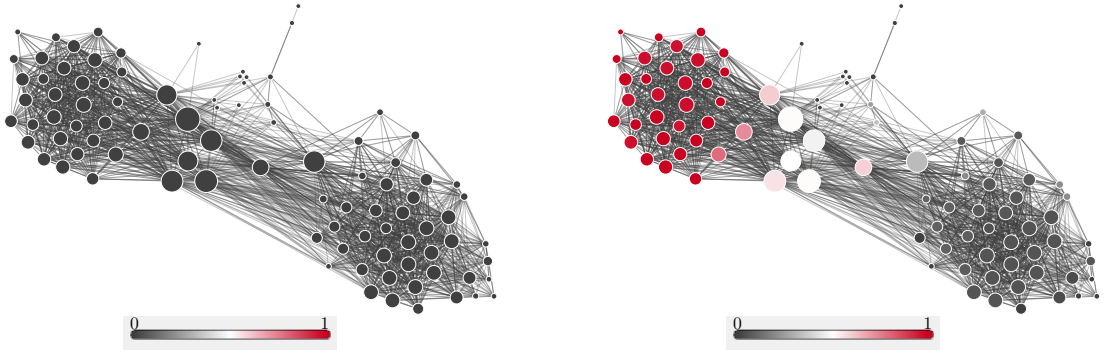

(a) $S_{\mathscr{B}} = 0.19$ (b) $S_{\mathscr{B}} = 0.07$

(c) $S_{\mathscr{B}} = 0.08$ (d) $S_{\mathscr{B}} = 0.66$

FIG. 6. Example final activation patterns (*i.e.* network states) for the Macaque network on 95 nodes along with their respective basin stabilities. Here $P = 1.1$ and solutions shown are those with basin stability scores of at least 5%. As well as the 'down' state (a) and the 'up' state (d), we have two non-trivial intermediate states (b, c) whose activity is driven by the modular structure of the network. While prominent in the directed connectome, the intermediate states of (b, c) have negligibly small basins of attraction in the corresponding undirected connectome.

the sustainability (or network robustness) of said states. We find that network patterns are typically organised according to the modular architecture of the underlying structural network as demonstrated in Figure 6 for the Macaque connectome on 95 nodes. This finding has important implications since the modularity structure of the undirected and empirical networks can differ markedly. As mentioned previously, the inclusion of false positive connections can effect a break-down in the modular topology of the network as modules merge to form new larger modules, which possibly explains the observed increase in neural activity for the undirected connectomes in this study (see figures 4 and 5). This type of hyper-activity is reminiscent of the types of excessive synchronisation found in many neurological disorders and perhaps hints at the important role network directionality plays in network mechanisms underlying healthy spreading dynamics. We emphasise again, that the results displayed in Figure 6 are representative of the solutions obtained across all four connectomes considered in this work. (Results omitted for brevity.)

We note, that the influence of network modularity in the formation of neural activity patterns observed in this study is similar to recently reported results implicating network modularity in the formation of network patterns via Turing mechanisms (50). In this study, the authors used both numerical and analytical techniques to explore pattern formation on modular networks with their key results being that (a) modularity is crucial for the self-organisation of the global dynamics on a network; and (b) based on their studies (as well as recent results in (51)), significantly richer dynamics are expected in the case of directed networks, such as the emergence of travelling Turing waves, which importantly, are not observed in the undirected case. We note here, that the effect of directionality on the pattern formation capabilities of modular, connectome-based networks is an open area of research.

We remark that our results are in contrast to the study by Golos *et al.* (17) in which observed numbers of attractor states were orders of magnitude higher than found here, even for the case of the micro-scale *C. elegans* connectome; however, it is important to note that the connectomes studied in (17) are of the order $n = 1000$ and that the number of attractor states of (2.1) scale with network complexity (as seen in the case of *C. elegans*). Also, whilst the number of attractor states was much larger in the study by Golos *et al.*, a closer analysis determined a small set of 'significant' (and importantly comparably sized) activity patterns resembling observed resting state networks in the human brain. Other recent studies (52; 53) have reported attractor landscapes populated by a small number of patterns, as in this study, whilst results from empirical investigations typically posit the existence of up to eight different sustainable network patterns. (See, for example, the paper by Damoiseaux *et al.* (54).) The critical brain hypothesis (55) states that neuronal dynamics are governed by a dynamical system close to criticality. The resting state networks (*i.e.* attractor states) of this dynamical system are then multistable ghost attractors that shape the global dynamics of the system. Importantly, results in this study indicate that directed network topology can have a strong influence on both the number *and* configuration of admissible network patterns.

To conclude, in this study we have shown that network directionality can profoundly impact the information capacity of connectome-based networks. Thus the inability of modern neuroimaging techniques to resolve connection directionality can potentially lead to substantial errors in the classification of network patterns making it difficult to define a meaningful dynamical repertoire (*i.e.* collection of prototypical brain states) of the brain. In future studies, we shall extend the current work to consider the affect that network directionality has on large-scale brain dynamics in the case when the local node dynamics is governed by a more sophisticated neural population model capable of exhibiting complex oscillatory behaviours (*e.g.* the neural mass models of Jasen and Ritt (6) or Coombes and Byrne (56)). This is an important next step since recent work by Forrester *et al.* (57) found that whilst structure clearly facilitates observed functional connectivity patterns in the brain, the degree with which it influ-

ences said patterns is determined by the dynamics of its neural subunits. Another natural extension of the work presented here is to deduce the extent to which directed network structure impacts on functional connectivity matrices (*i.e.* inferred from correlated activity between nodes) of the brain. In a series of recent papers Moon *et al.* (58; 59) demonstrated that changes in directionality patterns across states of human consciousness are driven by alterations of brain network topology. Importantly, in the aforementioned studies network directionality was unaccounted for (largely due to the use of diffusion tensor imaging techniques to reconstruct connectome representations) and so it would be of great interest to extend these ideas to include structural directionality (where possible) in order to determine the extent to which these directed patterns of functional connectivity are altered.

Acknowledgment

AP would like to acknowledge Nottingham Trent University for funding via a Vice-Chancellor's PhD Scholarship.

References

[1] Viktor Jirsa, Olaf Sporns, Michael Breakspear, Gustavo Deco, and Anthony Randal McIntosh. Towards the virtual brain: network modeling of the intact and the damaged brain. *Archives italiennes de biologie*, 148(3):189–205, 2010.

[2] Stephen Coombes. Large-scale neural dynamics: simple and complex. *NeuroImage*, 52(3):731–739, 2010.

[3] Danielle S Bassett, Perry Zurn, and Joshua I Gold. On the nature and use of models in network neuroscience. *Nature Reviews Neuroscience*, 19(9):566–578, 2018.

[4] Kanika Bansal, Johan Nakuci, and Sarah Feldt Muldoon. Personalized brain network models for assessing structure–function relationships. *Current opinion in neurobiology*, 52:42–47, 2018.

[5] Hugh R Wilson and Jack D Cowan. Excitatory and inhibitory interactions in localized populations of model neurons. *Biophysical journal*, 12(1):1–24, 1972.

[6] Ben H Jansen and Vincent G Rit. Electroencephalogram and visual evoked potential generation in a mathematical model of coupled cortical columns. *Biological cybernetics*, 73(4):357–366, 1995.

[7] Olivier David and Karl J Friston. A neural mass model for meg/eeg:: coupling and neuronal dynamics. *NeuroImage*, 20(3):1743–1755, 2003.

[8] Melissa Zavaglia, Filippo Cona, and Mauro Ursino. A neural mass model to simulate different rhythms in a cortical region. *Computational intelligence and neuroscience*, 2010, 2010.

[9] Mikail Rubinov, Olaf Sporns, Cees van Leeuwen, and Michael Breakspear. Symbiotic relationship between brain structure and dynamics. *BMC neuroscience*, 10(1):55, 2009.

[10] Gustavo Deco, Adrián Ponce-Alvarez, Dante Mantini, Gian Luca Romani, Patric Hagmann, and Maurizio Corbetta. Resting-state functional connectivity emerges from structurally and dynamically shaped slow linear fluctuations. *Journal of Neuroscience*, 33(27):11239–11252, 2013.

[11] Michael Breakspear. Dynamic models of large-scale brain activity. *Nature neuroscience*, 20(3):340, 2017.

[12] Joana Cabral, Morten L Kringelbach, and Gustavo Deco. Exploring the network dynamics underlying brain activity during rest. *Progress in neurobiology*, 114:102–131, 2014.

[13] Christian F Beckmann, Marilena DeLuca, Joseph T Devlin, and Stephen M Smith. Investigations into resting-state connectivity using independent component analysis. *Philosophical Transactions of the Royal Society B: Biological Sciences*, 360(1457):1001–1013, 2005.

[14] Cristina Rosazza and Ludovico Minati. Resting-state brain networks: literature review and clinical applications. *Neurological sciences*, 32(5):773–785, 2011.

[15] Enrique CA Hansen, Demian Battaglia, Andreas Spiegler, Gustavo Deco, and Viktor K Jirsa. Functional connectivity dynamics: modeling the switching behavior of the resting state. *Neuroimage*, 105:525–535, 2015.

[16] JA Scott Kelso. Multistability and metastability: understanding dynamic coordination in the brain. *Philosophical Transactions of the Royal Society B: Biological Sciences*, 367(1591):906–918, 2012.

[17] Mathieu Golos, Viktor Jirsa, and Emmanuel Daucé. Multistability in large scale models of brain activity. *PLoS computational biology*, 11(12):e1004644, 2015.

[18] Penelope Kale, Andrew Zalesky, and Leonardo L Gollo. Estimating the impact of structural directionality: How reliable are undirected connectomes? *Network Neuroscience*, 2(02):259–284, 2018.

[19] Martijn P van den Heuvel and Olaf Sporns. Network hubs in the human brain. *Trends in cognitive sciences*, 17(12):683–696, 2013.

[20] Stuart Oldham and Alex Fornito. The development of brain network hubs. *Developmental cognitive neuroscience*, 36:100607, 2019.

[21] Danielle S Bassett, Edward Bullmore, Beth A Verchinski, Venkata S Mattay, Daniel R Weinberger, and Andreas Meyer-Lindenberg. Hierarchical organization of human cortical networks in health and schizophrenia. *Journal of Neuroscience*, 28(37):9239–9248, 2008.

[22] Mikail Rubinov et al. Schizophrenia and abnormal brain network hubs. *Dialogues in clinical neuroscience*, 15(3):339, 2013.

[23] Jérémy Guillon, Yohan Attal, Olivier Colliot, Valentina La Corte, Bruno Dubois, Denis Schwartz, Mario Chavez, and F De Vico Fallani. Loss of brain inter-frequency hubs in alzheimer's disease. *Scientific reports*, 7(1):1–13, 2017.

[24] Uri Alon. Network motifs: theory and experimental approaches. *Nature Reviews Genetics*, 8(6):450–461, 2007.

[25] Leonardo L Gollo and Michael Breakspear. The frustrated brain: from dynamics on motifs to communities and networks. *Philosophical Transactions of the Royal Society B: Biological Sciences*, 369(1653):20130532, 2014.

[26] Leonardo L Gollo, Claudio Mirasso, Olaf Sporns, and Michael Breakspear. Mechanisms of zero-lag synchronization in cortical motifs. *PLoS computational biology*, 10(4), 2014.

[27] Leonardo L Gollo, James A Roberts, and Luca Cocchi. Mapping how local perturbations influence systems-level brain dynamics. *Neuroimage*, 160:97–112, 2017.

[28] Marc Timme. Revealing network connectivity from response dynamics. *Physical review letters*, 98(22):224101, 2007.

[29] Víctor M Eguíluz, Toni Pérez, Javier Borge-Holthoefer, and Alex Arenas. Structural and functional networks in complex systems with delay. *Physical Review E*, 83(5):056113, 2011.

[30] Emily SC Ching and HC Tam. Reconstructing links in directed networks from noisy dynamics. *Physical Review E*, 95(1):010301, 2017.

[31] John J Hopfield. Neurons with graded response have collective computational properties like those of two-state neurons. *Proceedings of the national academy of sciences*, 81(10):3088–3092, 1984.

[32] Peter J Menck, Jobst Heitzig, Norbert Marwan, and Jürgen Kurths. How basin stability complements the linear-stability paradigm. *Nature physics*, 9(2):89–92, 2013.

[33] Klaas Enno Stephan. The history of cocomac. *Neuroimage*, 80:46–52, 2013.

[34] JW Scannell, GAPC Burns, CC Hilgetag, MA O'Neil, and Malcolm P Young. The connectional organization of the cortico-thalamic system of the cat. *Cerebral Cortex*, 9(3):277–299, 1999.

[35] Richard Michael Durbin. Studies on the development and organisation of the nervous system of caenorhabditis elegans, 1987.

[36] John G White, Eileen Southgate, J Nichol Thomson, and Sydney Brenner. The structure of the nervous system of the nematode caenorhabditis elegans. *Philos Trans R Soc Lond B Biol Sci*, 314(1165):1–340, 1986.

[37] Mikail Rubinov and Olaf Sporns. Complex network measures of brain connectivity: uses and interpretations. *Neuroimage*, 52(3):1059–1069, 2010.

[38] Yoonsuck Choe, BH McCormick, and W Koh. Network connectivity analysis on the temporally augmented c. elegans web: A pilot study. In *Soc Neurosci Abstr*, volume 30, 2004.

[39] Marcus Kaiser and Claus C Hilgetag. Nonoptimal component placement, but short processing paths, due to long-distance projections in neural systems. *PLoS computational biology*, 2(7):e95, 2006.

[40] Daniel J Felleman and DC Essen Van. Distributed hierarchical processing in the primate cerebral cortex. *Cerebral cortex (New York, NY: 1991)*, 1(1):1–47, 1991.

[41] Edward H Yeterian and Deepak N Pandya. Corticothalamic connections of the posterior parietal cortex in the rhesus monkey. *Journal of Comparative Neurology*, 237(3):408–426, 1985.

[42] ST Carmichael and JL Price. Architectonic subdivision of the orbital and medial prefrontal cortex in the macaque monkey. *Journal of Comparative Neurology*, 346(3):366–402, 1994.

[43] James W Lewis and David C Van Essen. Mapping of architectonic subdivisions in the macaque monkey, with emphasis on parieto-occipital cortex. *Journal of Comparative Neurology*, 428(1):79–111, 2000.

[44] F Reinoso-Suarez. Connectional patterns in parietotemporooccipital association cortex of the feline cerebral cortex. *Cortical integration. IBRO*, 11:255–278, 1984.

[45] Jack W Scannell, Colin Blakemore, and Malcolm P Young. Analysis of connectivity in the cat cerebral cortex. *Journal of Neuroscience*, 15(2):1463–1483, 1995.

[46] Ernesto Estrada. *The structure of complex networks: theory and applications*. Oxford University Press, 2012.

[47] Olaf Sporns and Richard F Betzel. Modular brain networks. *Annual review of psychology*, 67:613–640, 2016.

[48] Lucianoda F Costa, Marcus Kaiser, and Claus C Hilgetag. Predicting the connectivity of primate cortical networks from topological and spatial node properties. *BMC systems biology*, 1(1):16, 2007.

[49] Alice Rokszin, Zita Márkus, Gábor Braunitzer, Antal Berényi, György Benedek, and Attila Nagy. Visual pathways serving motion detection in the mammalian brain. *Sensors*, 10(4):3218–3242, 2010.

[50] Bram A Siebert, Cameron L Hall, James P Gleeson, and Malbor Asllani. The role of modularity in self-organisation dynamics in biological networks. *arXiv preprint arXiv:2003.12311*, 2020.

[51] Malbor Asllani, Joseph D Challenger, Francesco Saverio Pavone, Leonardo Sacconi, and Duccio Fanelli. The theory of pattern formation on directed networks. *Nature communications*, 5(1):1–9, 2014.

[52] Gustavo Deco, Mario Senden, and Viktor Jirsa. How anatomy shapes dynamics: a semi-analytical study of the brain at rest by a simple spin model. *Frontiers in computational neuroscience*, 6:68, 2012.

[53] Gustavo Deco and Viktor K Jirsa. Ongoing cortical activity at rest: criticality, multistability, and ghost attractors. *Journal of Neuroscience*, 32(10):3366–3375, 2012.

[54] Jessica S Damoiseaux, SARB Rombouts, Frederik Barkhof, Philip Scheltens, Cornelis J Stam, Stephen M Smith, and Christian F Beckmann. Consistent resting-state networks across healthy subjects. *Proceedings of the national academy of sciences*, 103(37):13848–13853, 2006.

[55] Luca Cocchi, Leonardo L Gollo, Andrew Zalesky, and Michael Breakspear. Criticality in the brain: A synthesis of neurobiology, models and cognition. *Progress in neurobiology*, 158:132–152, 2017.

[56] Stephen Coombes and Aine Byrne. Next generation neural mass models. In *Nonlinear Dynamics in Computational Neuroscience*, pages 1–16. Springer, 2019.

[57] Michael Forrester, Jonathan J Crofts, Stamatios N Sotiropoulos, Stephen Coombes, and Reuben D O'Dea. The role of node dynamics in shaping emergent functional connectivity patterns in the brain. *Network Neuroscience*, 4(2):467–483, 2020.

[58] Joon-Young Moon, UnCheol Lee, Stefanie Blain-Moraes, and George A Mashour. General relationship of global topology, local dynamics, and directionality in large-scale brain networks. *PLoS computational biology*, 11(4), 2015.

[59] Joon-Young Moon, Junhyeok Kim, Tae-Wook Ko, Minkyung Kim, Yasser Iturria-Medina, Jee-Hyun Choi, Joseph Lee, George A Mashour, and UnCheol Lee. Structure shapes dynamics and directionality in diverse brain networks: mathematical principles and empirical confirmation in three species. *Scientific reports*, 7:46606, 2017.